Petroleum Science 19 (2022) 1516–1526

Contents lists available at ScienceDirect

Petroleum Science

journal homepage: www.keaipublishing.com/en/journals/petroleum-science

Original Paper

The effect of the density difference between supercritical CO_2 and supercritical CH_4 on their adsorption capacities: An experimental study on anthracite in the Qinshui Basin

Si-Jie Han [a, b], Shu-Xun Sang [a, b, c, *], Piao-Piao Duan [c, **], Jin-Chao Zhang [c], Wen-Xin Xiang [c], Ang Xu [c]

[a] Jiangsu Key Laboratory of Coal-based Greenhouse Gas Control and Utilization, China University of Mining and Technology, Xuzhou, Jiangsu, 221008, China
[b] Carbon Neutrality Institute, China University of Mining and Technology, Xuzhou, Jiangsu, 221008, China
[c] School of Resources and Geosciences, China University of Mining and Technology, Xuzhou, Jiangsu, 221116, China

ARTICLE INFO

Article history:
Received 9 January 2021
Accepted 25 January 2022
Available online 4 March 2022

Edited by Jie Hao

Keywords:
CO_2 geological storage
Competitive adsorption
Deep unmineable coal
Average number of layers of adsorbed molecules
Density ratio between free phase and adsorbed phase
Micropore filling

ABSTRACT

Deep unmineable coals are considered as economic and effective geological media for CO_2 storage and CO_2 enhanced coalbed methane (CO_2-ECBM) recovery is the key technology to realize CO_2 geological sequestration in coals. Anthracite samples were collected from the Qinshui Basin and subjected to mercury intrusion porosimetry, low-pressure CO_2 adsorption, and high-pressure CH_4/CO_2 isothermal adsorption experiments. The average number of layers of adsorbed molecules (ANLAM) and the CH_4/CO_2 absolute adsorption amounts and their ratio at experimental temperatures and pressures were calculated. Based on a comparison of the density of supercritical CO_2 and supercritical CH_4, it is proposed that the higher adsorption capacity of supercritical CO_2 over supercritical CH_4 is the result of their density differences at the same temperature. Lastly, the optimal depth for CO_2-ECBM in the Qinshui Basin is recommended. The results show that: (1) the adsorption capacity and the ANLAM of CO_2 are about twice that of CH_4 on SH-3 anthracite. The effect of pressure on the CO_2/CH_4 absolute adsorption ratio decreases with the increase of pressure and tends to be consistent. (2) A parameter (the density ratio between gas free and adsorbed phase (DRFA)) is proposed to assess the absolute adsorption amount according to the supercritical CO_2/CH_4 attributes. The DRFA of CO_2 and CH_4 both show a highly positive correlation with their absolute adsorption amounts, and therefore, the higher DRFA of CO_2 is the significant cause of its higher adsorption capacity over CH_4 under the same temperature and pressure. (3) CO_2 adsorption on coal shows micropore filling with multilayer adsorption in the macro-mesopore, while methane exhibits monolayer surface coverage. (4) Based on the ideal CO_2/CH_4 competitive adsorption ratio, CO_2 storage capacity, and permeability variation with depth, it is recommended that the optimal depth for CO_2-ECBM in the Qinshui Basin ranges from 1000 m to 1500 m.

1. Introduction

In the context of China's coal-dominated energy structure, CCUS (carbon capture, utilization, and storage) technology is an important part of the country's large-scale carbon emissions reduction strategy, which aims to achieve carbon neutrality by 2060. Of the different geological storage methods, CO_2 storage enhanced coalbed methane (CO_2-ECBM) is considered to be an important pathway for achieving both carbon emissions reduction and the efficient development of CBM since the injected CO_2 displaces methane from CH_4-bearing coal seams in the process of being stored (Yang et al., 2015; Liu et al., 2019). Although a few studies have suggested that CH_4 has stronger interactions with coal compared to CO_2 at low pressures (Busch et al., 2006), most studies regarding the competitive adsorption of CO_2/CH_4 mixtures on coals

* Corresponding author. Jiangsu Key Laboratory of Coal-based Greenhouse Gas Control and Utilization, China University of Mining and Technology, Xuzhou, Jiangsu, 221008, China.
** Corresponding author.
E-mail addresses: shxsang@cumt.edu.cn (S.-X. Sang), duanpiaopiao@163.com (P.-P. Duan).

https://doi.org/10.1016/j.petsci.2022.03.003

indicate that it is CO_2 which has the higher adsorption capacity (e.g. Tang et al., 2004; Dai et al., 2009; Weniger et al., 2012; Zhou et al., 2013a; Luo et al., 2018). In these studies, the CO_2/CH_4 adsorption ratio varies from 1 to 10, and a relative decrease in the adsorption ratio with the increase of coal rank has also been observed (Busch and Gensterblum, 2011). The adsorption selectivity of CO_2/CH_4 is affected by moisture, vitrinite content, temperature, gas concentration, pressure, and other factors (Busch et al., 2006; Ottiger et al., 2008; Weishauptová et al., 2015). Although these influencing factors have different ways of acting on adsorption selectivity, the root causes of CO_2/CH_4 competitive adsorption are their various gas-soil interaction mechanisms under different environmental conditions. The higher adsorption of CO_2 over CH_4 on coal has been attributed to the reasons such as: (1) gas-coal interactions and (2) the thermodynamic properties of the gases (Milewska-Duda et al., 2000; Cui et al., 2004; Harpalani et al., 2006; Sakurovs et al., 2010; Zhang et al., 2015; Jin et al., 2017). The smaller molecular diameter of CO_2 (0.33 nm) versus CH_4 (0.38 nm) also favors the entry of the former into the micropores in the coal structure. CO_2 uptake in coal is a combination of adsorption and absorption; hence, the amount of CO_2 adsorbed is higher than that of CH_4 (Milewska-Duda et al., 2000). The results of quantum chemistry and molecular simulations indicate that the Van der Waals' forces between CO_2 and coal are stronger than those between CH_4 and coal (Harpalani et al., 2006; Sakurovs et al., 2010). Molecular simulation is a powerful tool to investigate gas adsorption behavior on coal, especially to properly explain the controlling effect of pore size and functional groups on the competitive adsorption of multi-component gases (Mosher et al., 2013; Dong et al., 2019). Molecular simulation results exhibit the effects of different influencing factors on CO_2/CH_4 competitive adsorption and provide strong evidence for CO_2's preferential adsorption on coal over CH_4 based on the molecular dynamics theory (Asif et al., 2019; Zhou et al., 2019; Long et al., 2021). The test and modeling results from the CO_2-ECBM pilot in the Qinshui Basin indicate that CO_2 injection can significantly improve CBM recovery, but can also lead to problems such as unstable gas production and a lower-than-expected amount of stored CO_2 (Ye et al., 2012, 2016; Zhou et al., 2013b). Generally, CO_2 and CH_4 are both in a supercritical state in deep coal reservoirs (> 1000 m) but however show significant differences in their free gas density due to changes in temperature and pressure. These results indicate that a variety of supercritical gas adsorption behaviors are induced on coal owing to the dramatic density changes in supercritical gases (Do and Do, 2003; Sakurovs et al., 2007; Gensterblum et al., 2013; Song et al., 2015; Han et al., 2019). However, few, if any, studies have focused on the precise relationship between the density of supercritical gas and its adsorption onto coals. Hence, it is unclear whether gas density contributes to the preferential adsorption of supercritical CO_2 on coal over CH_4 under the same reservoir conditions. To investigate this, it is necessary to conduct a comparative study on the different adsorption capacities of the two gases under the same reservoir conditions from the perspective of their different supercritical density attributes.

Against this backdrop, the present study utilized mercury intrusion porosimetry (MIP) and low-pressure CO_2 adsorption (LPCA) techniques to investigate pore size distributions and pore structure parameters of SH-3 anthracite in the Qinshui Basin. High-pressure CO_2/CH_4 isothermal adsorption experiments were carried out at different temperatures. The differences in the adsorption isotherms of the two gases were evaluated from the perspective of the differences in the gas density and a parameter, which is defined as a density ratio between the free and adsorbed phases (DRFA), was proposed to compare adsorption behavior between supercritical CO_2 and CH_4. The modified Dubinin-Radushkevich (MDR) adsorption model was then applied to interpret the CO_2/CH_4 adsorption behavior in coal. Finally, considering ideal geological CO_2 storage conditions, a potential depth range was recommended for CO_2-ECBM in the Qinshui Basin.

2. Samples and methods

2.1. Sample

The SH-3 anthracite investigated in this work was collected from the No.3 coal seam of the Shanxi Formation in the Sihe coalfield in the Qinshui Basin. The SH-3 anthracite was received in particle sizes ranging from fine powders to large particles of 50 mm in diameter from the same working face. Representative samples were obtained by coning and quartering, and crushing and screening methods were employed to obtain the required size ranges for the experiments. The samples were initially flushed with nitrogen gas and stored in a thick, vacuum-sealed polyethylene container that was placed in a desiccator. Vitrinite reflectance, proximateand maceral analyses were conducted according to the Chinese national standards GB/T 6948–2008, GB/T 8899-2013, and GB/T212-2008, and the results are summarized in Table 1. The coal size and quality required by the different experiments in this study are shown in Table 2.

2.2. Determination of pore structure parameters

MIP measurements were conducted on anthracite with a particle size of 1–3 mm using an AutoPore IV 9510 instrument (Micromeritics, USA), with both degassing and intrusion being automatically controlled by the supplied software. During the MIP measurement, which was conducted according to the Chinese national standard GB/T 21650.1–2008, the samples were pressurized from 0.0099 to 413.46 MPa and the mercury contact angle and surface tension during intrusion were assumed to be 130° and 0.485 $N \bullet m^{-1}$ (Okolo et al., 2015), respectively. The CO_2 surface

Table 1
Results of proximate analyses and maceral analyses.

Sample No.	R_o, %	Vitrinite, Vol.%	Inertinite, Vol.%	M_{ad}, wt.%	A_{ad}, wt.%	VM_{daf}, wt.%	FC_{ad}, wt.%
SH-3	3.10	79.84	18.36	2.21	12.77	5.62	79.46

Annotation: R_o-vitrinite reflectance, M-moisture content, A-ash content, VM-volatile content, FC-fixed carbon content.

Table 2
Sample sizes and quality for the different experiments.

Methods	Vitrinite reflectance	Maceral statistics	Proximate analysis	MIP	LPCA	High pressure CH_4/ CO_2 adsorption
Size, mm	0.45–1		0.15–0.2	1–3	0.28–0.45	0.18–0.25
Quality, g	30		30	10	20	100

areas and porosity properties of the samples were determined using an Autosorb-IQ-MP surface area and porosity analyzer (Quantachrome, USA). The samples (~20 g) were degassed under vacuum at 90 °C for 48 h prior to the adsorption analysis (0 °C in an ice bath). Adsorption data were acquired in the relative pressure range of $0 < P/P_0 < 0.032$. LPCA was conducted according to the Chinese national standard GB/T 21650.3–2011.

2.3. High-pressure CO_2/CH_4 isothermal adsorption experiments

To compare the differences of adsorption between CH_4 and CO_2 at a given temperature, high-pressure gas adsorption experiments were conducted using the manometric method. Prior to the drying process, the coal samples (as received) were crushed to particle sizes ranging from 60 to 80 mesh (0.18 to 0.25 mm) and then preserved in a vacuum bag. The adsorption experiments were carried out using 100 g coal samples that were dried at 105 °C in a vacuum drying oven for 1.5 h before being rapidly weighed and transferred to the adsorption cell. Prior to the adsorption isotherm measurements, the void volumes of the adsorption cell with and without the coal sample were determined using helium (99.999%) due to its non-adsorptive nature. The experimental temperatures were 40 °C, 50 °C, 60 °C, 70 °C, and 80 °C, and the maximum equilibrium pressures were 12 MPa for CH_4 and 16 MPa for CO_2. The maximum equilibrium pressure for CO_2 was higher since the large changes in the CO_2 adsorption curves at high pressures required the measurement of more data points to improve the fitting accuracy. The high-pressure adsorption isotherm experiments were carried out according to the Chinese national standard GB/T 19560-2008.

The adsorption amounts obtained from the manometric method are excess adsorption amounts. For low-pressure gas adsorption, the difference between the excess adsorption amount and the absolute adsorption amount is negligible, but for high-pressure gas adsorption, especially for high-pressure CO_2 adsorption, their difference is significant. Therefore, the analysis of supercritical CO_2 adsorption should be based on absolute adsorption. Excess adsorption is defined as the net amount of gas adsorbed on a sorbent without gas of free density, and the absolute adsorption can be calculated from the following equation:

$$n_a = \frac{n_{exc}}{(1 - \rho_g/\rho_a)} \tag{1}$$

where n_a is the absolute adsorption amount, (mmol/g), n_{exc} is the excess adsorption amount, (mmol/g), ρ_g is the free gas density (cm^3/g), ρ_a is the adsorbed gas density (1.0 g/cm^3 for CO_2 and 0.42 g/cm^3 for CH_4 (Day et al., 2008; Tang et al., 2017)).

2.4. MDR adsorption model

Previous studies have shown that gas adsorption on coals mainly occurs in micropores (Moore, 2012; Feng et al., 2017; Wang et al., 2017). The widely-used micropore filling methods, such as the Dubinin-Astakhov (D-A) and Dubinin-Radushkevich (D-R) models, tend to adopt saturated vapor pressure; however, this pressure loses its physical significance for supercritical gas. Therefore, instead of equilibrium pressure and saturated vapor pressure, Sakurovs et al. (2007) employed the free- and adsorbed-phase densities, respectively. In addition, an empirical parameter, k, was introduced to establish a modified D-R (or MDR) adsorption equation based on the D-R model:

$$n_{exc} = n_0\left(1 - \frac{\rho_g}{\rho_a}\right)e^{-D\left[\ln\left(\rho_a/\rho_g\right)\right]^2} + k\rho_g \tag{2}$$

where n_0 is the adsorption capacity, D is a function of both the heat of adsorption and the affinity of the gas for coal, and k is the correction coefficient related to adsorption swelling.

2.5. Calculation of the average number of layers of adsorbed molecules (ANLAM)

In addition to adsorption capacity, the number of layers of adsorbed molecules is also a measure of a gas's adsorption behavior. For the assessment of adsorbed gas molecules, Zhou et al. (2003) proposed an equation to calculate the ANLAM as follows:

$$V_a = A_a\left[1\Big/\left(10^{-3}\rho_a Av\right)\right]^{1/3}\lambda \tag{3}$$

where V_a is the maximum volume of the adsorbed phase (calculated from the maximum absolute adsorption capacity), A is the specific surface area (SSA) of the adsorbent, ρ_a is the density of the adsorbed phase, Av is Avogadro's number (6.022×10^{23}), and λ is the average number of adsorbate layers.

3. Results

3.1. Pore structure parameters

The results of the pore structure parameters of the SH-3 anthracite determined using the MIP and LPCA methods are summarized in Fig. 1 and Table 3. The pore size distribution of the SH-3 anthracite determined by the different methods has good continuity and the distributions of pore volume and pore surface area are similar. The pore volume and surface area decrease as pore size

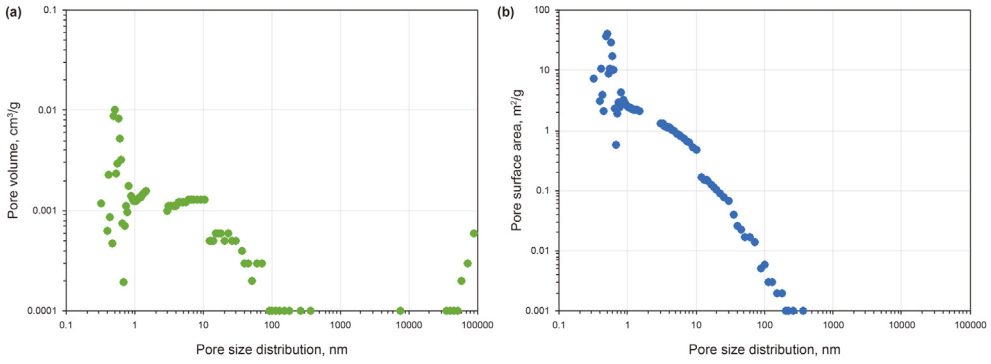

Fig. 1. Pore size distribution of the SH-3 anthracite determined by the MIP and LPCA methods. (**a**) Pore volume; (**b**) Specific surface area.

Table 3
Results of pore structure parameters determined by different measuring methods.

Method	Parameter	SH-3
MIP	Pore volume, cm^3/g	0.045
	Total specific surface area, m^2/g	5.44
	Average pore size, nm	32.80
	Porosity, %	6.41
	Apparent density, g/mL	1.44
	Skeletal density, g/mL	1.54
LPCA	DFT pore volume, cm^3/g	0.069
	DFT specific surface area, m^2/g	224.98
	DFT average pore size, nm	0.50

increases and their maximums occur between 0.5 and 0.6 nm. However, there is a weak peak near 0.1 μm in Fig. 1a, indicating the development of micro-fractures. The MIP results show that the pore sizes were >3 nm, i.e., meso-macropores, with a pore volume of 0.045 cm^3/g, an SSA of 5.44 m^2/g, and an average pore size of 32.8 nm. The pore size range determined via LPCA was 0.3–1.8 nm, i.e. micropores, with a pore volume of 0.069 cm^3/g, an SSA of 224.98 m^2/g, and an average pore size of 0.5 nm. These results indicate that the SH-3 anthracite has a stronger development of micropores since the pore size ranges determined by MIP and LPCA were completely different, with no overlap whatsoever. In addition, the SSA value obtained from LPCA was >40 times greater than that from MIP; therefore, it is evident that the available SSA for gas adsorption is mostly provided by the microporosity of the coal.

3.2. High-pressure CH_4/CO_2 adsorption isotherms

The experimental results of the high-pressure adsorption of CH_4 and CO_2 are shown in Fig. 2, in which the CH_4 adsorption isotherms show obvious Langmuir-like behavior, with the adsorption amounts negatively correlated with temperature. However, the CO_2 adsorption isotherms all showed maximum excess adsorption amounts in the range of 6–10 MPa. In addition, these maxima were shifted to the right at higher temperatures. The adsorption isotherms at different temperatures all intersected, and the intersection points also tended to shift rightwards with increasing temperature. The excess adsorption amounts of CO_2 were negatively correlated with temperature at low pressures but showed an opposite trend at high pressures. At the experimental pressure range, the maximum excess adsorption amounts of CH_4 at elevated temperatures were 1.08, 1.05, 0.97, 0.85, and 0.72 mmol/g, respectively, while those of CO_2 at the corresponding temperatures were nearly twice as large, which were 2.12, 1.94, 1.79, 1.66, and 1.59 mmol/g, respectively.

3.3. Fitting of the MDR adsorption model

The results of fitting the MDR adsorption model to the high-pressure adsorption data of the CO_2 and CH_4 are shown in Table 4. As the table shows, all the R^2 values for all the fits were >99%, indicating that the model can accurately characterize the adsorption behavior for both the supercritical gases on coals. The adsorption capacities of supercritical CH_4 on coal ranged from 1.17 to 1.65 mmol/g, which is significantly lower than those of supercritical CO_2 at the same temperature (2.49–3.06 mmol/g). Although the adsorption capacities of both gases decreased with increasing temperature, as expected, the CO_2/CH_4 adsorption ratio ranged from 1.85 to 2.2, with no significant temperature dependence observed. The values of D (from Eq. (1)) for the supercritical adsorption data were also not obviously correlated with the temperature, with those for CO_2 being lower at all temperatures except at 70 °C. This anomaly may be related to the slight changes in the temperature of the adsorption cell during the experiments. The k values for the supercritical CH_4 were positive and uncorrelated with temperature, while those for the supercritical CO_2 were negative and decreased with increasing temperature. This may be interpreted as being due to a higher swelling induced by CO_2 adsorption, which caused a larger reduction in the adsorption amount.

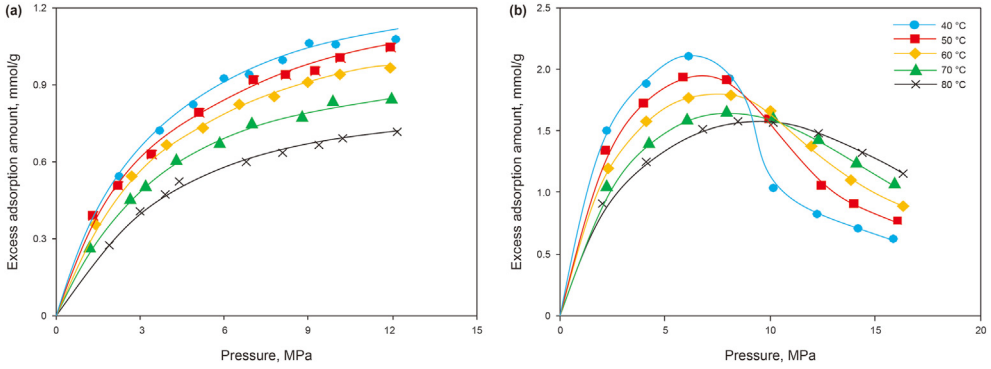

Fig. 2. Isothermal adsorption curves at different temperatures (the fitted lines are calculated by the MDR adsorption model). (**a**) CH_4; (**b**) CO_2.

Table 4
The fitted results of the high-pressure CH_4/CO_2 adsorption on the SH-3 anthracite.

Gas	CH_4				CO_2				Adsorption ratio
Temperature, °C	n_0, mmol/g	D	k	R^2	n_0, mmol/g	D	k	R^2	
40	1.65	0.095	0.65	0.992	3.06	0.066	−0.02	0.998	1.85
50	1.30	0.082	2.59	0.996	2.87	0.066	−0.05	0.997	2.20
60	1.27	0.081	2.02	0.998	2.72	0.072	−0.13	0.992	2.15
70	1.28	0.093	0.76	0.995	2.56	0.096	−0.13	0.995	1.99
80	1.17	0.098	0.03	0.994	2.49	0.082	−0.17	0.996	2.13

Table 5
ANLAMs of CH_4/CO_2 and their MPSCGFs in the SH-3 anthracite at different temperatures.

Gas	Temperature, °C	Adsorption capacity, mmol/g	ANLAM	MPSCGF, nm
CH_4	40	1.65	0.70	0.53
	50	1.30	0.55	0.42
	60	1.27	0.53	0.40
	70	1.28	0.54	0.41
	80	1.17	0.49	0.37
CO_2	40	3.06	1.42	0.94
	50	2.87	1.33	0.88
	60	2.72	1.26	0.83
	70	2.56	1.19	0.79
	80	2.49	1.16	0.77

3.4. Calculation of the ANLAM

The pore sizes of SH-3 anthracite from MIP and LPCA were completely different, with the former technique being used mainly to investigate macro- and meso-pores, while the latter mainly representingmicropores. The results showed that the SSA of the micropores was significantly 40 times larger than that of the macro-mesopores, making the latter negligible in terms of gas adsorption, which is consistent with the adsorption potential theory due to the narrower pore sizes of micropores. The adsorption potential on the micropore surface is larger than that on the macroporous surface due to the superposition of the adsorption potential on the relative pore wall, which causes the adsorbate molecules to preferentially occupy the micropore adsorption sites; therefore, the assumption that the SSA of micropores can be considered as the total SSA was applied when calculating the ANLAM using Eq. (2). The results of the ANLAM and the maximum pore sizes for complete gas filling (MPSCGF) are listed in Table 5.

Table 5 shows that the ANLAM values for CO_2 and CH_4 were significantly different, and both were negatively correlated with temperature. The ANLAM of CH_4 ranged from 0.49 to 0.7, indicating that the adsorption state of CH_4 on coal consists of unsaturated monolayer surface coverage, which is typical of monolayer adsorption; however, that of CO_2 ranged from 1.16 to 1.42, indicating full surface coverage for the first layer, and unsaturated surface coverage for the second or third layer (i.e., multi-layer adsorption). The MPSCGF ranges of CO_2 and CH_4 were 0.77–0.94 nm and 0.37–0.53 nm, respectively, suggesting that the pore sizes that can be completely filled by CO_2 are about twice as large as those for CH_4, which helps to explain the significantly higher adsorption capacity of CO_2 over CH_4 on coal.

4. Discussion

4.1. Comparison of supercritical CO_2/CH_4 adsorption on coal

The fitted results from the MDR adsorption model show that, within the experimental conditions used, the supercritical CO_2 absolute adsorption amounts on the SH-3 anthracite are higher than those of the supercritical CH_4 (Fig. 3a). The adsorption curve shapes of CO_2 and CH_4 are also significantly different. The absolute adsorption curves of CH_4 are close to linear, and the increasing rate of the adsorption amount at low pressure is slightly higher than that at high pressure. In contrast, the slopes of the CO_2 adsorption curves before and after the critical pressure are quite different. Below the critical pressure of CO_2, the adsorption amounts show a rapid increase, while at high pressures, the increasing rate of the adsorption amount significantly reduces and the curve shapes of CO_2 are similar to those of CH_4. In addition, the ratio of the absolute adsorption amounts (CO_2/CH_4) can be divided into two distinct stages: at pressures <2 MPa, the initial absolute adsorbed amounts of the two gases varied greatly, but these differences decreased sharply with increasing pressure. At pressures >2 MPa, this ratio decreased slowly with increasing pressure, gradually approaching 2 (Fig. 3b). These results suggest a decreasing effect of pressure on the CO_2/CH_4 absolute adsorption ratio, which is consistent with the results of previous molecular simulation studies (Zhang et al., 2015). The ultimate ratio of 2 indicates that twice the number of CO_2 molecules can be held at a given adsorption site compared with CH_4. At low pressures, the ratio was >2, which increased significantly as the pressure decreased due to the fact that CO_2 micropore filling occurs at low pressures, while CH_4 molecules interact weakly with coal and only form a monolayer on the surface. However, as the pore size increases, the adsorption potential cannot continue to be superimposed on the relative pore wall, which results in no adsorption in the pore centers; hence, volume filling is not sustainable at high pressure. This leads to surface-only adsorption of CO_2 molecules in unfilled pores at high pressure, thereby significantly reducing the growth of CO_2 adsorption amount. In addition, most of the available adsorption sites in coal are occupied by CO_2 molecules at low pressure. Therefore, under the combined action of these two phenomena, the ratio of the absolute adsorbed amount gradually decreases with increasing pressure until the surface is saturated.

4.2. Supercritical CO_2 and CH_4 density attributes

The NIST REFPROP software package was used to calculate the free-phase densities of CO_2 and CH_4 as functions of temperature and pressure and these results are shown in Fig. 4a. As the figure

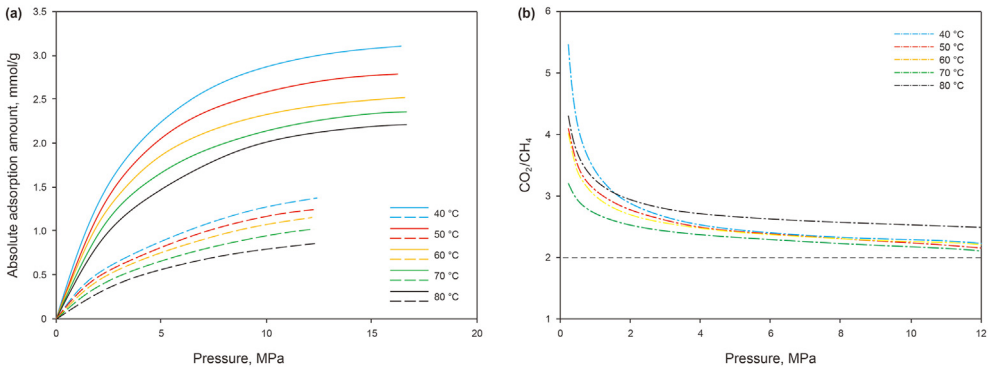

Fig. 3. (**a**) Fitted results of the CH_4/CO_2 absolute adsorption amount on the SH-3 anthracite at different temperatures (dotted line: CH_4; solid line: CO_2); (**b**) Ratio of the absolute adsorption amount between CO_2 and CH_4.

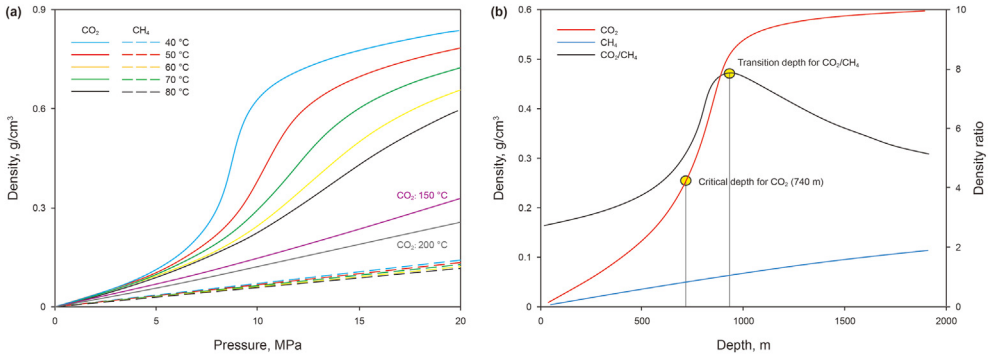

Fig. 4. (**a**) Density changes of CO_2/CH_4 with the increase in pressure at different temperatures; (**b**) the density of CO_2 and CH_4 under coal reservoir environments in the Qinshui Basin.

shows, the CH_4 density is relatively small, and increases nearly linearly with pressure, while not showing a visible temperature dependence. The CO_2 density is controlled by both temperature and pressure, especially near its critical point. The lower the temperature, the more obvious the variation of the density of CO_2 near the critical point. For example, at 40 °C, the CO_2 density increased almost vertically near 8 MPa. However, as the temperature increased, not only did the CO_2 density at a given pressure decrease, but the increase in density also became stagnant, suggesting that the variation of CO_2 density was inhibited by the high temperature. To better understand this attribute of supercritical CO_2, curves of the CO_2 density at 150 °C and 200 °C were also calculated. The results show that at these temperatures, the CO_2 density showed a linear increase similar to that of CH_4, and the density curves were also closer to CH_4. Therefore, it is speculated that when the temperature is high enough, the changes in CO_2 density are similar to those of CH_4. This phenomenon can be interpreted by considering the high critical temperature of CO_2. The experimental temperature is close to the critical temperature of CO_2, but it is much higher than the critical temperature of CH_4; hence, under the experimental conditions, the gases exhibit different fluid densities and different changes in density, which result in their free-phase densities being quite different in real reservoir environments. For a better comparison, the CO_2 and CH_4 density curves were calculated at depths ranging from 0 to 2000 m, as found in the Qinshui Basin (Fig. 4b). The results show that the CH_4 density curve is similar to that in Fig. 4a, but the CO_2 density curve only resembles that at low temperature (for example, 40°C), which suggests that the change in CO_2 density plays a significant role in its adsorption behavior in actual reservoir environments. The free-phase density ratio between CO_2 and CH_4 shows a maximum value with the depth of ~950 m. After the depth is greater than 950 m, the increase in CO_2 density slows down considerably, implying that the effect of supercritical CO_2 density on adsorption is reduced at greater depths.

According to the adsorption potential theory, the gas adsorbed on the pore surfaces of coal is in a highly condensed state due to the interactions between the gas and coal. The adsorbed phase density is high on the coal's surface, but decreases with increasing distance from the pore surface, due to the weakening of the adsorption potential, until it is equal to the free-phase density in the pore centers. Based on this, the closer the free- and adsorbed-phase densities, the greater the gas density at the boundary between the adsorbed and free phases, resulting in an increase in the adsorbed amount. Therefore, once a certain temperature is fixed, an increase in the free-phase density directly induces an increase in the number of gas molecules in the adsorption space. This process is explained intuitively in Fig. 5. Hence, the relative sizes of the free- and adsorbed-phase densities can reflect the increase or decrease in the adsorbed amount caused by changes in the gas density. Accordingly, a critical parameter for assessing the amount of gas adsorbed on coals, DRFA, is proposed here.

The DRFA values for CO_2 and CH_4 as a function of pressure and temperature are shown in Figs. 6a and b. As the figure shows, the DRFA of CO_2 has a clearer temperature dependence. The lower the temperature, the faster the DRFA of CO_2 increases near the critical pressure. The DRFA of CH_4 showed a linear increase, which was significantly smaller than that of CO_2, and was not significantly affected by temperature (Fig. 6b). In general, the DRFA of CO_2/CH_4 showed a peak value that decreased with increasing temperature. When the temperature was 80 °C, the DRFA increased monotonically with pressure (Fig. 6c). Under the experimental conditions, the DRFA of CO_2 was greater than that of CH_4 and the maximum ratio of the DRFA between CO_2 and CH_4 approached 3.78 at the temperature of 40 °C. In the range of 15–20 MPa, the

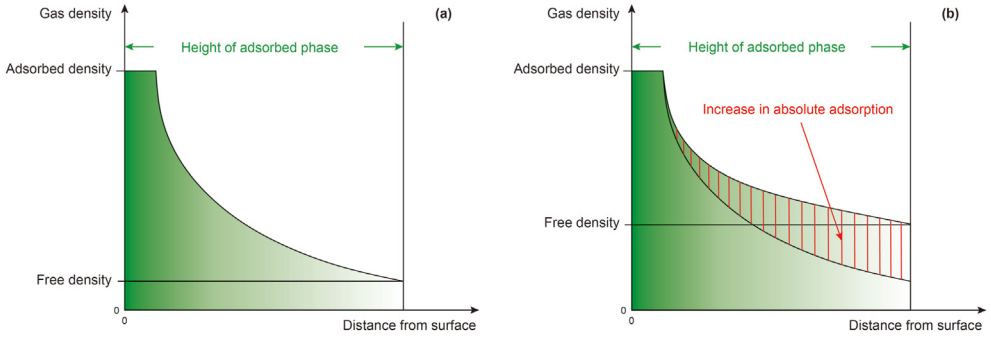

Fig. 5. Effect of free phase density on adsorption capacity. (**a**) Low free phase density; (**b**) After an increase in density.

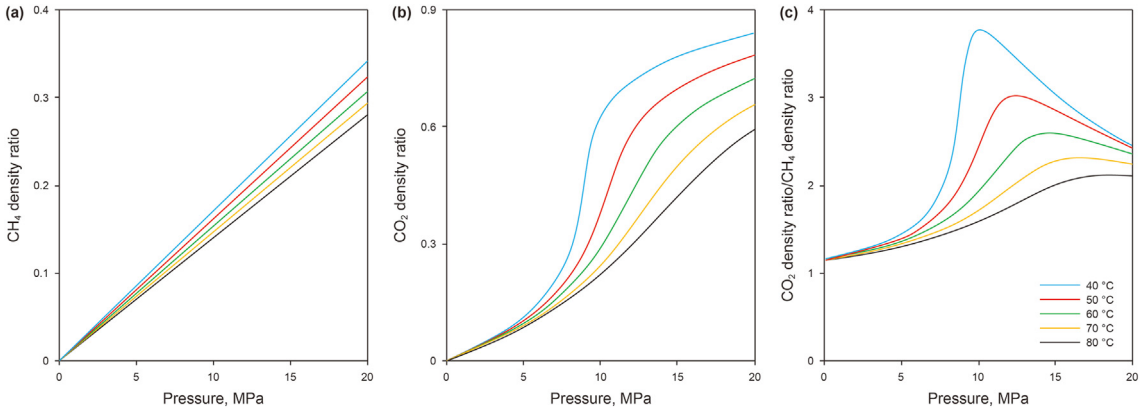

Fig. 6. The CO_2/CH_4 density ratio between the free phase density and the adsorbed phase density with the increase in pressure at different temperatures. (**a**) DRFA of CO_2; (**b**) DRFA of CH_4; (**c**) The ratio of DRFA between CO_2 and CH_4.

DRFA of CO_2 was over twice that of CH_4. Compared to the difference in the free-phase density between the two gases in Fig. 3, the DRFA of CH_4 is closer to that of CO_2 as a whole. For example, at 20 MPa, the DRFA of CH_4 was ~0.3, while the actual CH_4 free-phase density was <0.15 g/cm^3. This is because the CH_4 adsorbed phase density is less than that of CO_2. Moreover, the DRFA not only intuitively reveals the gas density differences between CO_2 and CH_4 at different temperatures and pressures but also reflects the relative sizes of the free- and adsorbed-phase densities. The large differences in DRFA at different temperatures are due to the supercritical CO_2/CH_4 attributes. Previous studies have shown that supercritical CO_2 exhibits an obvious two-phase attribute including a gas-like phase and a liquid-like phase but that as the temperature increases, this two-phase attribute fades away (Simeoni et al., 2010; Artemenko et al., 2017). In fact, the critical temperature of CH_4 is low, and it shows no such two-phase attribute under the experimental conditions; therefore, the DRFA ratio between the two gases basically reflects the drastic change of the supercritical CO_2 density near the critical conditions. In addition, it may be inferred from the trend in DRFA that at the experimental temperature, the ratio approaches 2 at infinite pressure. This value is consistent with the corresponding ratio of the absolute adsorption capacity, suggesting that the DRFA is a key factor in determining the adsorption capacity of coal towards different gases.

4.3. Gas density-induced differences in adsorption capacity

To better understand the gas density effect on adsorption, the changes in the absolute adsorbed amounts of CO_2 and CH_4 with DRFA at different pressures were further calculated (Fig. 7). The results show that the absolute adsorption capacities of both gases show a strongly positive linear correlation with the DRFA, confirming the inference from section 4.2 that the DRFA values of gases determine their adsorption capacities. In addition, Fig. 7 also reveals that within the ranges of the experimental temperature and pressure, the DRFA of CH_4 was always lower than that of CO_2, and there was a significant difference in the growth rate (slope) of the absolute adsorbed amount between the two gases. The absolute adsorbed amount of subcritical CO_2 increased rapidly with the DRFA, and its growth rate decreased significantly as the CO_2 entered the supercritical state. Although the growth rate of the absolute adsorbed amount of CH_4 also decreased with increasing pressure, this decrease was significantly smaller than that for CO_2. This is because the change in the DRFA of CH_4 was smaller than that of CO_2 under the experimental temperature and pressure, especially owing to the significant difference in the CO_2 density around the critical point. These results not only illustrate the high adsorption capacity of CO_2 resulting from its high DRFA, but also reflect the weakening of the contribution of supercritical CO_2 to the increase in the absolute adsorption capacity at high pressures; therefore, the difference in the DRFA values between CO_2 and CH_4 directly indicates their different adsorption capacities on coals.

The ANLAM intuitively indicates that the difference in the adsorbed amount of the different gases is closely related to the DRFA. This is because the higher the DRFA, the closer the free- and adsorption-phase densities and the shorter the distance between gas molecules in the free phase, which allows more free-phase molecules to enter the adsorption space, thereby increasing the number of adsorbed molecular layers. As the adsorption potential range on the pore surface of a given coal is fixed, it is the number of adsorbate molecules in the adsorption space that determines the adsorption capacity. Due to the low critical temperature of CH_4, the DRFA of supercritical CH_4 is small and does not change appreciably under reservoir conditions. At reservoir pressures, the intermolecular distance of the free-phase CH_4 is not sufficient for it to enter the adsorption potential range. This limits the increase in the ANLAM, resulting in the adsorbed CH_4 maintaining a monolayer state. After a short but rapid increase in the adsorption amount of CH_4 at low density resulting from the strong adsorption potential in the micropore, monolayer surface coverage dominates the contribution on the increase of the CH_4 adsorption amount (Fig. 8a). In contrast, since the critical temperature of CO_2 is close to the coal reservoir's temperature, the free-phase CO_2 density changes drastically with pressure, resulting in a large change in DRFA and ANLAM. In addition, since CO_2 has a higher DRFA, its free-phase intermolecular distances are closer to those in the adsorption phase, facilitating capture by the pore surface and increasing the possibility of multi-molecular layer adsorption (Fig. 8b). The formation of multilayer adsorption inevitably leads to an increase in the upper limit of pore sizes that can be completely filled with gas and then the larger micropore is completely filled. Therefore, compared to CH_4, the contribution of micropore filling on the increase of the CO_2 adsorption amount is more durable at high gas densities. The calculated results also show that the pore sizes that can be completely filled by CH_4 range from 0.37 to 0.53 nm, which is similar to the average pore size (0.5 nm) of the SH-3 anthracite, whereas the corresponding pore size range for CO_2 of 0.77–0.94 nm is significantly larger than the preponderant micropore size distribution of the SH-3 anthracite (0.3–0.65 nm). Accordingly, it can be concluded that due to their different adsorption behaviors, supercritical CO_2 exhibits a combination of micropore filling and multilayer surface coverage, and a high DRFA

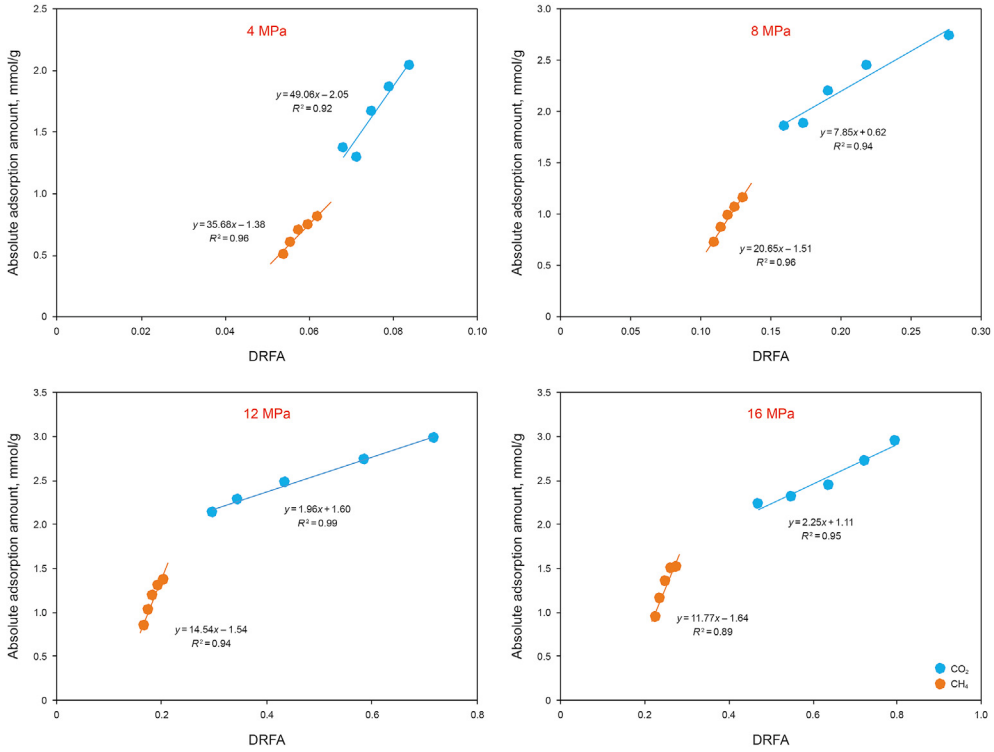

Fig. 7. Relationship between the absolute adsorption of CH_4/CO_2 and their density ratio at various pressures.

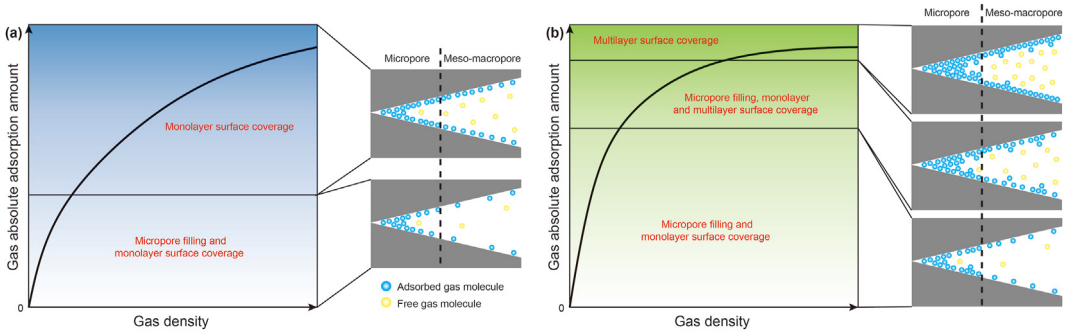

Fig. 8. Gas adsorption models on coal as gas density increases and the contribution of different gas adsorption behaviors on the increasing of the gas adsorption amount. (**a**) CH_4; (**b**) CO_2.

contributes to the appearance of the multilayer adsorption at high pressures. Furthermore, CH_4 always shows monolayer adsorption with minor volume filling in the small micropores. As a result, the adsorption capacity of CO_2 is greater than that of CH_4 under the same reservoir conditions.

4.4. Implications for CO_2-ECBM

In coal reservoirs, the gradual increase in temperature and pressure with depth results in significant changes in the CO_2 density during CO_2 injection into deep unmineable coal seams. In this study, the Qinshui Basin was taken as an example to calculate the absolute adsorbed amount of CO_2 and CH_4 at different depths using the MDR adsorption model. The depths were calculated from the matching relation between the experimental temperatures and temperature gradient in the Qinshui Basin (the depth of the constant-temperature zone, at 15 °C, is 20 m), and the reservoir pressure gradient was assumed as 1 MPa/100 m. The results show that the maximum values of the absolute adsorbed amounts of CO_2 and CH_4 were 2.68 and 1.23 mmol/g, respectively, at depths of 1012 and 1295 m, respectively (Fig. 9a). These results, which are similar to those obtained in previous studies (Hildenbrand et al., 2006; Han et al., 2017), show that the occurrence of the maximum absolute adsorption amount is a result of the joint effects of DRFA and temperature. The adsorption capacities of CO_2 and CH_4 are negatively correlated with temperature (Fig. 9b); hence, the higher the temperature, the faster the adsorption capacity declines. On the one hand, the change rate of the DRFA value for CO_2 decreases gradually at greater depths (Fig. 9c), indicating that the DRFA has a smaller influence on the adsorbed amount of CO_2 in deeper reservoirs. On the other hand, the DRFA of CH_4 was positively correlated with depth, suggesting a more-or-less constant influence of the DRFA on the increase in the adsorption capacity. Accordingly, it may be concluded that as the depth increases, the effect of the DRFA of CO_2 is reduced, and the peak CO_2 adsorption is reached first, while due to the stable effect of the DRFA of CH_4, the maximum adsorbed amount of CH_4 lags behind that of CO_2 under the same reservoir conditions. These results demonstrate that the appropriate depth

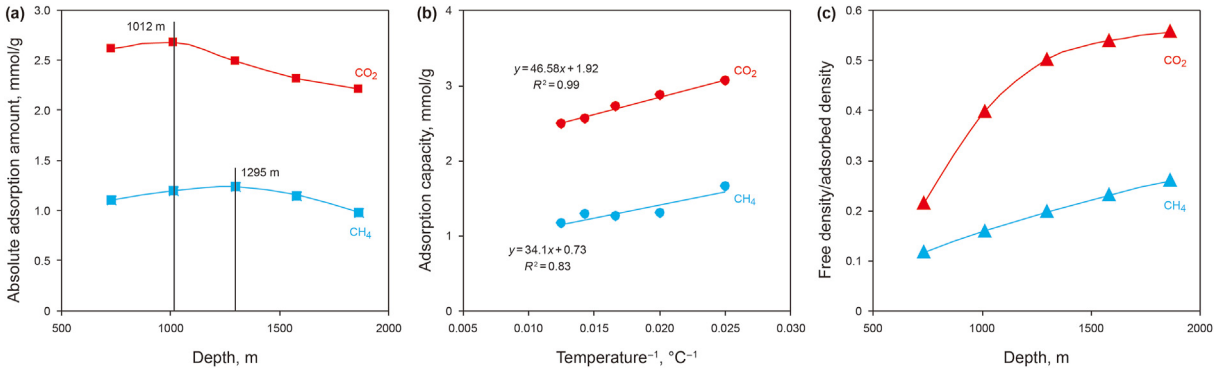

Fig. 9. (**a**) Changes of CO_2/CH_4 adsorption amount on SH-3 anthracite under the reservoir condition in the Qinshui Basin; (**b**) Relationship between the adsorption capacity of CO_2/CH_4 and temperature; (**c**) Changes in the CO_2/CH_4 density ratio under the reservoir condition in the Qinshui Basin.

for implementing geological CO_2 storage and enhanced CBM recovery should be separately considered as follows: (1) for geological CO_2 storage in the Qinshui Basin, the recommended depth is about 1000 m; (2) for CO_2-ECBM in the Qinshui Basin, CO_2/CH_4 competitive adsorption and the recoverable CBM reserves require extra consideration. Therefore the potential depth for CO_2-ECBM is expected to be greater than that for CO_2 storage alone.

Although in current CO_2-ECBM demonstrations, methane in coal cannot be completely replaced by injected CO_2, experimental and simulated results of CH_4 displacement by CO_2 in coals show that with the improvement of CO_2 injection technology, process, and efficiency, CH_4 displacement efficiency can reach 100% (Ranathunga et al., 2017; Fang et al., 2019). Therefore, the ideal CO_2/CH_4 competitive adsorption ratio (whereby CH_4 in coal seams is completely replaced by CO_2) can be used to theoretically evaluate the optimal depth for CO_2-ECBM projects. The ideal competitive adsorption ratio between CO_2 and CH_4 in coal seams showed a reverse parabola in the range of 500–2000 m, and its minimum value appeared at ~1500 m (Fig. 10a). A higher competitive adsorption ratio is conducive to the storage of CO_2. Under the coal reservoir conditions in the Qinshui Basin, the ideal CO_2/CH_4 competitive adsorption ratios above and below 1500 m both showed an increasing trend, but their increases have different reasons. The high ratio in the shallow part of the reservoir is due to the rapid increase in CO_2 adsorption capacity, while that in the deep part results from the decrease in the adsorption of CH_4. Taking the changes in CO_2 density and adsorption capacity with depth into consideration, it may be concluded that the shallow coal seams have both a high adsorption replacement ratio and a high CO_2 adsorption capacity. During CO_2-ECBM processes, permeability is the controlling factor for CO_2 injectability, and it decreases exponentially with increasing depth (Fig. 10b). Bachu et al. (2007) proposed that the permeability of coal for favorable CO_2 injection should be > 1 mD. A very low coal permeability is not conducive to CO_2 entering the pores from the cleat, resulting in injection failure or slow progress. Liu et al. (2020) also observed that after CO_2-coal interactions at the temperature and pressure conditions below 1500 m, the pore volume and surface area of coals showed a significant reduction, which plays a negative role in CO_2 geological storage. Therefore, from the perspective of enhancing the geological storage capacity of CO_2, CO_2 injectivity, and the CO_2/CH_4 replacement rate, CO_2 injection into coal seams at depths of 1000–1500 m appears to be more advantageous.

The CO_2 adsorption-induced swelling of coal plays a significant role in reducing its permeability, causing it to decrease by two orders of magnitude (Cui et al., 2007). A previous study indicated that the permeability of Qinshui Basin anthracite decreases by ~70% after supercritical CO_2 adsorption at 10 MPa and that the contribution of supercritical CO_2 adsorption to the permeability attenuation of coal is >30% (Niu et al., 2018); however, several studies have indicated that in the long term following CO_2 injection, the permeability of coal can recover or even increase as compared with its original value (Fujioka et al., 2010; Wei et al., 2010; Vishal et al., 2013). Hence, the original permeability of the coal and the variation in the relative permeability caused by injecting CO_2 are key factors in economically and efficiently implementing CO_2-ECBM projects.

At present, China has put forward the goal of reaching peak carbon emissions by 2030 and attaining carbon neutrality by 2060. Hence, the development and utilization of non-fossil energy sources and the reduction of CO_2 emissions have gradually become priority development paths in the fields of energy and resources, which inevitably requires the goal of CO_2-ECBM projects to shift

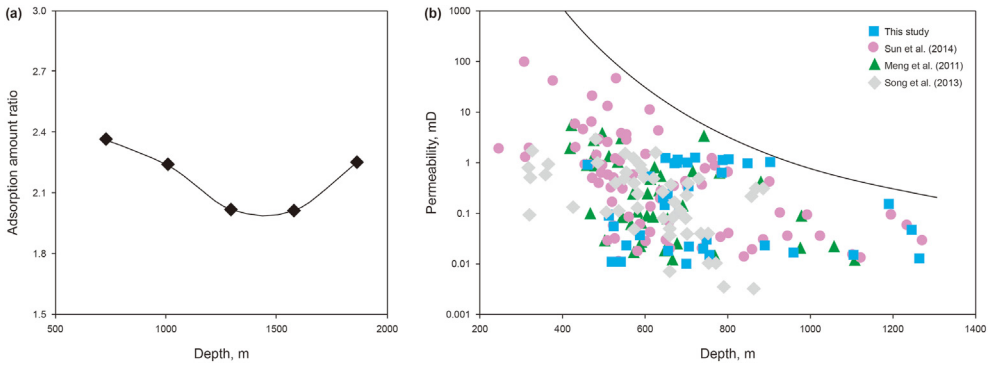

Fig. 10. (**a**) CO_2/CH_4 adsorption ration vs. depth under reservoir conditions of the Qinshui Basin; (**b**) Permeability vs. depth in the Qinshui Basin (Meng et al., 2011; Song et al., 2013; Sun et al., 2014).

focus from CBM development to the safe and efficient geological storage of CO_2. To this end, future research on CO_2-ECBM projects should prioritize finding the optimum depth and the structural or/and stratigraphic traps for geological CO_2 storage in different types of coal-bearing basins.

5. Conclusions

(1) The adsorption capacities of CH_4 on the SH-3 anthracite in this study ranged from 1.17 to 1.65 mmol/g and the ANLAMs ranged from 0.53 to 0.70, while for CO_2, the corresponding numbers were 2.49–3.06 mmol/g and 1.16–1.42, respectively. The ratio of the absolute adsorbed amount between CO_2 and CH_4 decreases with increasing pressure, and the adsorption capacity of CO_2 is about twice that of CH_4.

(2) CO_2 has a high critical temperature that is comparable to the experimental temperature; therefore, it presents a high density and shows rapid changes in its density near the critical point. CH_4 has a low density that shows a positive linear relationship with pressure. To better compare the absolute adsorption amount, a critical parameter (DRFA) is proposed according to the supercritical CO_2/CH_4 attributes. The DRFA shares a high affinity with the ANLAM and determines the gas adsorption behavior in pores of different sizes.

(3) The higher DRFA of supercritical CO_2 is an important factor contributing to its greater adsorption capacity over CH_4. The DRFA values of CO_2 and CH_4 both show a positive relationship with the absolute adsorbed amounts. The high DRFA of CO_2 facilitates the entry of free CO_2 molecules in the adsorption space and the adsorbed CO_2 molecules fill the micropores as multilayer surface coverage, whereas CH_4 shows monolayer adsorption.

(4) As depth increased, the adsorbed amounts of CO_2 and CH_4 showed the maxima at depths of 1012 and 1295 m, respectively, in the Qinshui Basin. Considering CO_2 storage capacity, CO_2/CH_4 adsorption ratio, and permeability changes, the recommended depth range for CO_2-ECBM projects in the Qinshui Basin is 1000–1500 m. Future CO_2-ECBM projects should emphasize the geological storage of CO_2 in deep, unmineable coal seams under the pressure of carbon reduction, and the economic conditions, like the CO_2 injection speed, increment of CH_4 production, sources of CO_2 and carbon credit, etc., should also be considered.

Acknowledgements

We are very grateful to three anonymous reviewers for their constructive comments and helpful suggestions that significantly improved the original manuscript. The authors would like to acknowledge the financial support provided by National Natural Science Foundation of China (Nos. 42102207 and 42141012), Major Project supported by Jiangsu Key Laboratory of Coal-based Greenhouse Gas Control and Utilization, CUMT (2020ZDZZ01C), the Fundamental Research Funds for the Central Universities (2021YCPY0106) and A Project Funded by the Priority Academic Program Development of Jiangsu Higher Education Institution (PAPD).

References

Artemenko, S., Krijgsman, P., Mazur, V., 2017. The Widom line for supercritical fluids. J. Mol. Liq. 238, 122–128. https://doi.org/10.1016/j.molliq.2017.03.107.

Asif, M., Naveen, P., Panigrahi, D.C., et al., 2019. Adsorption isotherms of CO_2-CH_4 binary mixture using IAST for optimized ECBM recovery from sub-bituminous coals of Jharia coalfield: an experimental and modeling approach. Int. J. Coal.Prep.Util. 39 (8), 1–18. https://doi.org/10.1080/19392699.2019.1626842.

Bachu, S., Bonijoly, D., Bradshaw, J., et al., 2007. CO_2 storage capacity estimation: methodology and gaps. Int. J. Greenh. Gas Control 1 (4), 430–443. https://doi.org/10.1016/S1750-5836(07)00086-2.

Busch, A., Gensterblum, Y., 2011. CBM and CO_2-ECBM related sorption processes in coal: a review. Int. J. Coal Geol. 87 (2), 49–71. https://doi.org/10.1016/j.coal.2011.04.011.

Busch, A., Gensterblum, Y., Krooss, B.M., 2006. Investigation of high-pressure selective adsorption/desorption behaviour of CO_2 and CH_4 on coals: an experimental study. Int. J. Coal Geol. 66 (1/2), 53–68. https://doi.org/10.1016/j.coal.2005.07.003.

Cui, X., Bustin, R.M., Chikatamarla, L., 2007. Adsorption-induced coal swelling and stress: implications for methane production and acid gas sequestration into coal seams. J. Geophys. Res. Solid Earth 112 (B10), 1–16. https://doi.org/10.1029/2004JB003482.

Cui, X., Bustin, R.M., Dipple, G., 2004. Selective transport of CO_2, CH_4, and N_2 in coals: insights from modeling of experimental gas adsorption data. Fuel 83 (3), 293–303. https://doi.org/10.1016/j.fuel.2003.09.001.

Dai, S., Zhang, B., Zhu, C., et al., 2009. Isothermal adsorption of CH_4/CO_2 mixed gas for the late Paleozoic coals from the Kailuan coalfield of Hebei Province. J. China Coal Soc. 34 (5), 3–8 (in Chinese).

Day, S., Duffy, G., Sakurovs, R., et al., 2008. Effect of coal properties on CO_2 sorption capacity under supercritical conditions. Int. J. Greenh. Gas Control 2 (3), 342–352. https://doi.org/10.1016/S1750-5836(07)00120-X.

Do, D.D., Do, H.D., 2003. Adsorption of supercritical fluids in non-porous and porous carbons: analysis of adsorbed phase volume and density. Carbon 41 (9), 1777–1791. https://doi.org/10.1016/S0008-6223(03)00152-0.

Dong, K., Zeng, F., Jia, J., et al., 2019. Molecular simulation of the preferential adsorption of CH_4 and CO_2 in middle rank coal. Mol. Simulat. 45 (1), 15–25. https://doi.org/10.1080/08927022.2018.1521968.

Fang, H., Sang, S., Liu, S., et al., 2019. Experimental simulation of replacing and displacing CH_4 by injecting supercritical CO_2 and its geological significance. Int. J. Greenh. Gas Control 81, 115–125. https://doi.org/10.1016/j.ijggc.2018.12.015.

Feng, Z., Cai, T., Zhou, D., et al., 2017. Temperature and deformation changes in anthracite coal after methane adsorption. Fuel 192, 27–34. https://doi.org/10.1016/j.fuel.2016.12.005.

Fujioka, M., Yamaguchi, S., Nako, M., 2010. CO_2-ECBM field tests in the Ishikari coal basin of Japan. Int. J. Coal Geol. 82 (3–4), 287–298. https://doi.org/10.1016/j.coal.2010.01.004.

Gensterblum, Y., Merkel, A., Busch, A., et al., 2013. High-pressure CH_4 and CO_2 sorption isotherms as a function of coal maturity and the influence of moisture. Int. J. Coal Geol. 118, 45–57. https://doi.org/10.1016/j.coal.2013.07.024.

Han, S., Sang, S., Liang, J., et al., 2019. Supercritical CO_2 adsorption in a simulated deep coal reservoir environment, implications for geological storage of CO_2 in deep coals in the southern Qinshui Basin, China. Energy.Sci.Eng. 7 (2), 488–503. https://doi.org/10.1002/ese3.296.

Han, S., Sang, S., Zhou, P., et al., 2017. The evolutionary history of methane adsorption capacity with reference to deep Carboniferous-Permian coal seams in the Jiyang sub-basin: combined implementation of basin modeling and adsorption isotherm experiments. J. Petrol. Sci. Eng. 158, 634–646. https://doi.org/10.1016/j.petrol.2017.09.007.

Harpalani, S., Prusty, B.K., Dutta, P., 2006. Methane/CO_2 sorption modeling for coalbed methane production and CO_2 sequestration. Energy Fuels 20 (4), 1591–1599. https://doi.org/10.1021/ef0504341.

Hildenbrand, A., Krooss, B.M., Busch, A., 2006. Evolution of methane sorption capacity of coal seams as a function of burial history - a case study from the Campine basin, NE Belgium. Int. J. Coal Geol. 66 (3), 179–203. https://doi.org/10.1016/j.coal.2005.07.006.

Jin, Z., Wu, S., Deng, C., et al., 2017. Competitive adsorption behavior and mechanism of different flue gas proportions in coal. J. China Coal Soc. 42 (5), 1201–1206. https://doi.org/10.13225/j.cnki.jccs.2016.0997 (in Chinese).

Liu, C., Sang, S., Fan, X., Zhang, K., et al., 2020. Influences of pressures and temperatures on pore structures of different rank coals during CO_2 geological storage process. Fuel 259 (116273), 1–8. https://doi.org/10.1016/j.fuel.2019.116273.

Liu, C., Sang, S., Zhang, K., et al., 2019. Effects of temperature and pressure on pore morphology of different rank coals: implications for CO_2 geological storage. J. CO2 Util. 34, 343–352. https://doi.org/10.1016/j.jcou.2019.07.025.

Long, H., Lin, H., Yan, M., et al., 2021. Molecular simulation of the competitive adsorption characteristics of CH_4, CO_2, N_2, and multicomponent gases in coal. Powder Technol. 385 (1), 348–356. https://doi.org/10.1016/j.powtec.2021.03.007.

Luo, M., Li, S., Rong, H., et al., 2018. Experimental study on competitive adsorption relationship between CH_4 and N_2, CO_2 by NMR. J. China Coal Soc. 43 (2), 490–497. https://doi.org/10.13225/j.cnki.jccs.2017.1179 (in Chinese).

Meng, Z., Zhang, J., Wang, R., 2011. In-situ stress, pore pressure and stress-dependent permeability in the Southern Qinshui Basin. Int. J. Rock Mech. Min. Sci. 48 (1), 122–131.

Milewska-Duda, J., Duda, J., Nodzeński, A., et al., 2000. Absorption and adsorption of methane and carbon dioxide in hard coal and active carbon. Langmuir 16 (12), 5458–5466. https://doi.org/10.1021/la991515a.

Moore, T.A., 2012. Coalbed methane: a review. Int. J. Coal Geol. 101 (6), 36–81. https://doi.org/10.1016/j.coal.2012.05.011.

Mosher, K., He, J., Liu, Y., et al., 2013. Molecular simulation of methane adsorption in micro-and mesoporous carbons with applications to coal and gas shale systems.

Int. J. Coal Geol. 109, 36–44. https://doi.org/10.1016/j.coal.2013.01.001.
Niu, Q., Cao, L., Sang, S., et al., 2018. Experimental study of permeability changes and its influencing factors with CO_2 injection in coal. J. Nat. Gas Sci. Eng. 61, 215–225. https://doi.org/10.1016/j.jngse.2018.09.024.
Okolo, G.N., Everson, R.C., Neomagus, H.W., et al., 2015. Comparing the porosity and surface areas of coal as measured by gas adsorption, mercury intrusion and SAXS techniques. Fuel 141, 293–304. https://doi.org/10.1016/j.fuel.2014.10.046.
Ottiger, S., Pini, R., Storti, G., et al., 2008. Competitive adsorption equilibria of CO_2 and CH_4 on a dry coal. Adsorption 14, 539–556. https://doi.org/10.1007/s10450-008-9114-0.
Ranathunga, A.S., Perera, M.S.A., Ranjith, P.G., et al., 2017. Super-critical carbon dioxide flow behaviour in low rank coal: a meso-scale experimental study. J. CO2 Util. 20, 1–13. https://doi.org/10.1016/j.jcou.2017.04.010.
Sakurovs, R., Day, S., Weir, S., et al., 2007. Application of a modified Dubinin-Radushkevich equation to adsorption of gases by coals under supercritical conditions. Energy Fuels 21 (2), 992–997. https://doi.org/10.1021/ef0600614.
Sakurovs, R., Day, S., Weir, S., 2010. Relationships between the critical properties of gases and their high pressure sorption behavior on coals. Energy Fuels 24 (3), 1781–1787. https://doi.org/10.1021/ef901238c.
Simeoni, G.G., Bryk, T., Gorelli, F.A., et al., 2010. The Widom line as the crossover between liquid-like and gas-like behaviour in supercritical fluids. Nat. Phys. 6 (7), 503–507. https://doi.org/10.1038/nphys1683.
Song, Y., Liu, S., Ju, Y.W., et al., 2013. Coupling between gas content and permeability controlling enrichment zones of high abundance coal bed methane. Acta Pet. Sin. 34 (3), 417–426 (in Chinese).
Song, Y., Xing, W., Zhang, Y., et al., 2015. Adsorption isotherms and kinetics of carbon dioxide on Chinese dry coal over a wide pressure range. Adsorption 21 (1–2), 53–65. https://doi.org/10.1007/s10450-015-9649-9.
Sun, F., Wang, B., Li, M., et al., 2014. Major geological factors controlling the enrichment and high yield of coalbed methane in the southern Qinshui Basin. Acta Pet. Sin. 35 (6), 1070–1079 (in Chinese).
Tang, X., Ripepi, N., Luxbacher, K., et al., 2017. Adsorption models for methane in shales: review, comparison, and application. Energy Fuels 31 (10), 10787–10801. https://doi.org/10.1021/acs.energyfuels.7b01948.
Tang, S., Tang, D., Yang, Q., 2004. Variation regularity of gas component concentration in binary-component gas adsorption-desorption isotherm experiments. J. China Inst. Min. Technol. 33 (4), 86–90 (in Chinese).
Vishal, V., Ranjith, P.G., Singh, T.N., 2013. CO_2 permeability of Indian bituminous coals: implications for carbon sequestration. Int. J. Coal Geol. 105, 36–47. https://doi.org/10.1016/j.coal.2012.11.003.
Wang, S., Pan, J., Ju, Y., et al., 2017. The super-micropores in macromolecular structure of tectonically deformed coal using high-resolution transmission electron microscopy. J. Nanosci. Nanotechnol. 17 (9), 6982–6990. https://doi.org/10.1166/jnn.2017.14494.
Wei, X., Massarotto, P., Wang, G., et al., 2010. CO_2 sequestration in coals and enhanced coalbed methane recovery: new numerical approach. Fuel 89 (5), 1110–1118. https://doi.org/10.1016/j.fuel.2010.01.024.
Weishauptová, Z., Přibyl, O., Sýkorová, I., 2015. Effect of bituminous coal properties on carbon dioxide and methane high pressure sorption. Fuel 139, 115–124. https://doi.org/10.1016/j.fuel.2014.08.030.
Weniger, P., Franců, J., Hemza, P., et al., 2012. Investigations on the methane and carbon dioxide sorption capacity of coals from the SW Upper Silesian Coal Basin, Czech Republic. Int. J. Coal Geol. 93, 23–39. https://doi.org/10.1016/j.coal.2012.01.009.
Yang, H., Wang, Z., Ren, Z., 2015. Differences between competitive adsorption and replacement desorption of binary gases in coal and its replacement laws. J. China Coal Soc. 40 (7), 1550–1554. https://doi.org/10.13225/j.cnki.jccs.2014.1476 (in Chinese).
Ye, J., Zhang, B., Han, X., 2016. Well group carbon dioxide injection for enhanced coalbed methane recovery and key parameter of the numerical simulation and application in deep coalbed methane. J. China Coal Soc. 41 (1), 149–155. https://doi.org/10.13225/j.cnki.jccs.2015.9033 (in Chinese).
Ye, J., Zhang, B., Wong, S., 2012. Test of and evaluation on elevation of coalbed methane recovery ratio by injecting and burying CO_2 for 3# coal seam of north section of Shizhuang. Qingshui Basin, Shanxi. Engineering 2, 40–46 (in Chinese).
Zhou, L., Bai, S., Su, W., et al., 2003. Comparative study of the excess versus absolute adsorption of CO_2 on superactivated carbon for the near-critical region. Langmuir 19 (7), 2683–2690. https://doi.org/10.1021/la020682z.
Zhou, F., Hou, W., Allinson, G., et al., 2013b. A feasibility study of ECBM recovery and CO_2 storage for a producing CBM field in southeast Qinshui basin, China. Int. J. Greenh. Gas Control 19, 26–40. https://doi.org/10.1016/j.ijggc.2013.08.011.
Zhou, F., Hussain, F., Guo, Z., et al., 2013a. Adsorption/desorption characteristics for methane, nitrogen and carbon dioxide of coal samples from southeast Qinshui basin, China. Energy Explor. Exploit. 31 (4), 645–666. https://doi.org/10.1260/0144-5987.31.4.645.
Zhang, J., Liu, K., Clennell, M.B., et al., 2015. Molecular simulation of CO_2-CH_4 competitive adsorption and induced coal swelling. Fuel 160, 309–317. https://doi.org/10.1016/j.fuel.2015.07.092.
Zhou, W., Wang, H., Zhang, Z., et al., 2019. Molecular simulation of CO_2/CH_4/H_2O competitive adsorption and diffusion in brown coal. RSC Adv. 9 (6), 3004–3011. https://doi.org/10.1039/C8RA10243K.